ChemCatChem

Research Article
doi.org/10.1002/cctc.202300222

Chemistry Europe
European Chemical Societies Publishing

www.chemcatchem.org

Role of Titanium in Ti/SiO_2-Supported Metallocene-based Olefin Polymerization Catalysts. Part 2: Particle Fragmentation

Silvia Zanoni,[a] Nikolaos Nikolopoulos,[a] Alexandre Welle,[b] Virginie Cirriez,[b] and Bert M. Weckhuysen*[a]

A commercial SiO_2 modified by the addition of a TiO_2 layer on its surface and pore walls offers a support for metallocene-based ethylene polymerization catalysts with a 35% improved catalytic activity. The effect of such support modification on the catalyst particle fragmentation during polymerization reactions were assessed. This was performed by exposing the internal cross-section of several SiO_2 and Ti/SiO_2-based metallocene catalyst particles, polymerized at a wide range of reaction conditions, with a Focused-Ion Beam Scanning Electron Microscope (FIB-SEM), followed by a semi-quantitative analysis of polymer, catalyst and macropores of each 2D image obtained. The titanation of the SiO_2 lead to a support framework that fractures earlier and more efficiently. This was evidenced by the presence of several empty (polymer-free) cracks along the support dense-shell, found more extensively in the Ti-modified polymerized catalyst particle, which also resulted in a more sustained polymerized particles macroporosity during the course of the reaction.

Introduction

The support materials of heterogeneous olefin polymerization catalysts can have a great influence on their activity. Their morphology and mechanical strength affect the catalyst particle fragmentation process, while their surface species interact with the active sites, thereby influencing their intrinsic catalytic activity.[1] Hence, the choice of an appropriate support material for each specific olefin polymerization process is of high importance in the polymer manufacturing industry. Each support material has a unique resistance to the hydraulic forces produced by the accumulation of polymer, so a more friable $MgCl_2$ support of Ziegler–Natta catalysts generally fragments more rapidly than SiO_2 supports, often used in Phillips and metallocene-based polymerization catalysts.[2–4] The porosity of the support also affects the mechanical strength of the material as well as the diffusion of monomer through the catalyst particle.[5,6] For example, Lee and Choi studied the use of a pseudo-inverse opal silica as a support material with minimal intraparticle diffusion resistance, which showed both higher initial activity and a longer catalyst lifetime.[7] Similarly, smaller particles have shorter diffusion times with consequent higher polymerization activities.[8,9] Furthermore, the active sites can be impregnated on the support in various ways, with distributions that can be more or less homogenous throughout the support particle, another aspect having an effect on the catalyst fragmentation and the related polymerization activity.[10–13]

In $MgCl_2$-supported Ziegler–Natta catalyst materials, the fragmentation of the support might lead to the formation of new active sites as the breakage of clustered $TiCl_4$ in between $MgCl_2$ crystallites has been reported to create new Ti active centers.[14] On the other hand, in silica-based olefin polymerization catalysts no active sites are embedded in the support framework, as they are anchored on its surface. Hence, active sites aren't created when the support material fragments; rather, those that were not yet reached by the olefin monomer due to diffusion limitations can participate in the olefin polymerization reaction when new pathways are made throughout the catalyst particle fragmentation process.[3]

Metallocenes are generally supported on porous SiO_2 materials, which ensure a certain control over polymer particle morphology, while maintaining the tunability of their active center, a distinct characteristic of metallocenes over the other polymerization catalysts.[15–18] In our previous work, the fragmentation of a commercial silica-supported metallocene catalyst during ethylene polymerization was investigated with the use of a high-resolution Focused Ion Beam-Scanning Electron Microscope (FIB-SEM), for a series of reaction conditions.[19] It was found that this commercial catalyst fragmented in a layer-by-layer mode (Figure S1) where polymer material accumulated first, i.e., at the outer surface of the catalyst particle and on the walls of the support macropores. Furthermore, it was shown

[a] S. Zanoni, Dr. N. Nikolopoulos, Prof. B. M. Weckhuysen
Inorganic Chemistry and Catalysis group
Institute for Sustainable and Circular Chemistry and Debye Institute for Nanomaterials Science, Utrecht University
Universiteitsweg 99
3584 CG Utrecht (The Netherlands)
E-mail: b.m.weckhuysen@uu.nl
[b] Dr. A. Welle, Dr. V. Cirriez
Catalysis and Products R&D
TotalEnergies Petrochemicals
Zone Industrielle C
Seneffe-Feluy, 7181 (Belgium)

Supporting information for this article is available on the WWW under https://doi.org/10.1002/cctc.202300222

that bisectioning-like fracturing also occurred and that such phenomenon had a key role in allowing a complete fragmentation and continuous diffusion of monomer to the core of the silica support domains. In fact, the lack of bisectioning-like cracks leads to a less efficient fragmentation of the catalyst particle, as polymer accumulated at particles' surface and filled their macropores, slowing further diffusion of monomer and therefore decreasing the olefin polymerization rate. This phenomenon, i.e., insufficient bisectioning of the catalyst support, was observed in this commercial catalyst particles when polymerized in the gas-phase with high ethylene pressures, or in particles with initial low macroporosity. These findings underlined the necessity to select the right reaction conditions as well as the appropriate catalyst support, which is a topic thoroughly investigated in the literature for several olefin polymerization catalysts types and processes.[2,20–24]

Although generally not considered in the literature, the modification of a support material via grafting of different species on its surface, such as spacers or acidic sites, might also affect the fragmentation process of the particles during the olefin polymerization reaction. In part 1 of this study, we showed how the titanation of a commercial silica support material revealed to improve the catalytic activity of a supported metallocene-based ethylene polymerization catalyst.[25] The titanation procedure was shown to lead to a layer of TiO_2 grafted within the silica pores, ultimately reducing the pore volume of the modified catalyst compared to the commercial SiO_2-based one. The enhanced ethylene polymerization activity was primarily attributed to the presence of a second active site, namely reduced Ti^{3+} surface species, next to the primary Zr active site, thereby creating synergistic effects between the active centers, and to an overall higher Lewis acidity of the support thanks to the presence of 5-coordinated Ti^{4+} sites, which provided a higher activation efficiency of the Zr centers. For more details on the spectroscopic characterization of these materials which lead to such conclusions, the reader is referred to part 1 of this study.[25] Interestingly, the presence of Ti in the support material also caused an earlier onset of catalyst particle fragmentation, which was deduced from early-stage ethylene polymerization kinetic curves, although no polymerized catalyst particle was visually inspected. The question that arises here is whether the earlier catalyst fragmentation onset of the Ti-modified catalyst when compared to the commercial SiO_2-based catalyst could indeed be visualized, and to assess if such phenomenon occurs due to the higher activity of the modified catalyst material or if an altogether different catalyst fragmentation mechanism happens thanks to the presence of Ti species.

Hence, this study focuses on visualizing the difference in fragmentation between a commercial SiO_2-supported metallocene-based ethylene polymerization catalyst and the modified Ti/SiO_2-based one. This was done by first uncovering polymerized particles cross-sections with the use of Focused Ion Beam-Scanning Electron Microscopy (FIB-SEM) measurements and subsequently segmenting the so-obtained micrograms to assess the percentage composition of catalyst fragments, polymer material and macropores (see Figure 1 and *SI* for a more detailed explanation on the methodology).

The FIB-SEM methodology was selected over other techniques due to its accessibility and high resolution capabilities, which have been proven to enable the observation of subtle differences in sample fragmentation.[19] Although previous studies have utilized synchrotron-based x-ray tomography techniques to evaluate the fragmentation of other olefin

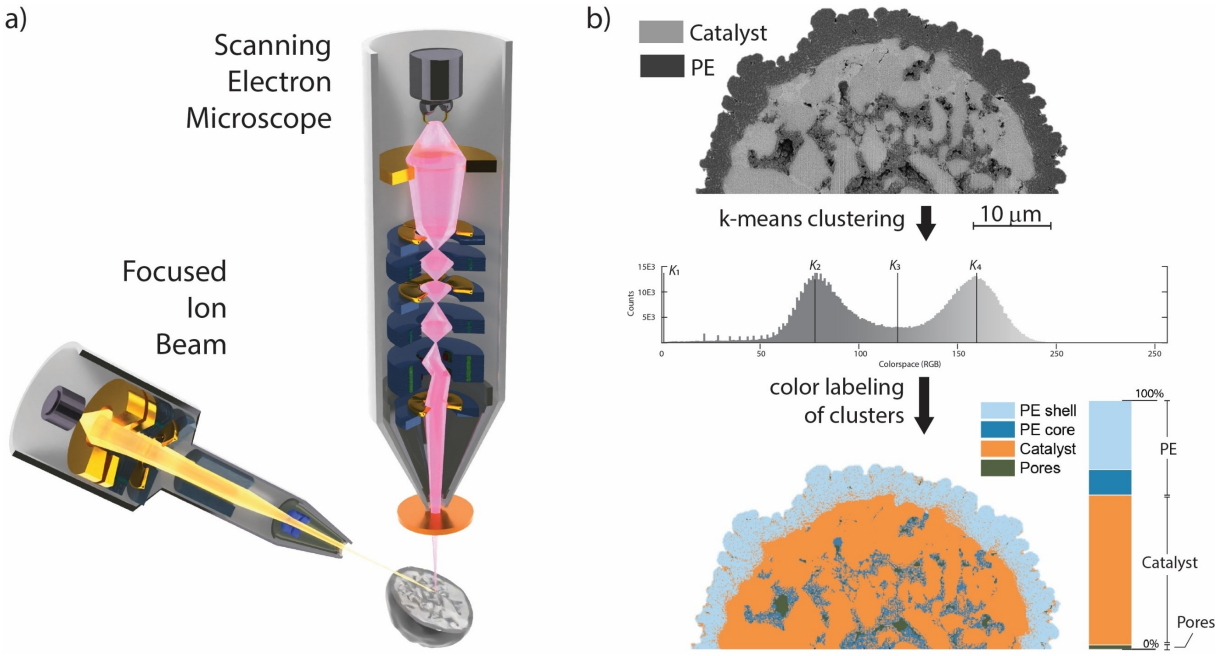

Figure 1. a) Schematic representation of a particle cross-section being exposed with a Focused Ion Beam-Scanning Electron Microscope (FIB-SEM). b) K-means image segmentation of the grey-scale cross section image.

polymerization catalysts, these techniques have limitations, such as longer measurement times and achieved resolutions dependent on sample stability under the x-ray beam, which still fall short of what can be achieved with high-resolution SEM.[26,27] Additionally, synchrotron data collection is less accessible than lab-based techniques, and evaluation of the measured sample is typically only possible after reconstruction of the dataset, a process that can be time-consuming and leaves little margin for error. On the contrary, SEM techniques allow for a screening of the polymerized catalyst batch and selection of a more representative particle sample to be analyzed. Thus, FIB-SEM was selected as the most practical and effective technique for comparing the expected subtle differences in fragmentation behavior across various reaction conditions between the Ti-modified catalyst and the commercial SiO_2-based catalyst.

The results obtained in this work, showed that the fragmentation of the two catalyst samples compared appeared to be occurring in a rather similar manner, i.e., in a layer-by-layer mode at the outer surface and at the walls of the macropores, as well as with the formation of bisectioning-like cracks within the catalyst particle. However, for the catalysts supported on the modified Ti/SiO_2, the bisectioning-type cracks appeared earlier and more extensively, causing a certain level of macroporosity to be maintained from the very beginning of the ethylene polymerization reaction, and that further increased as the reaction continued. As evidenced in a previous work based on the same commercial SiO_2-supported metallocene catalyst, this mode of fragmenting is essential for an efficient catalyst particle fragmentation and sufficient ethylene polymerization performance over the course of the reaction.[19] Hence, we can conclude that the presence of surface Ti species in this SiO_2 support positively affects the catalyst particle fragmentation by rendering the silica dense shell more prone to bisectioning-like fragmentation, therefore contributing to the higher ethylene polymerization activity of the catalyst material.

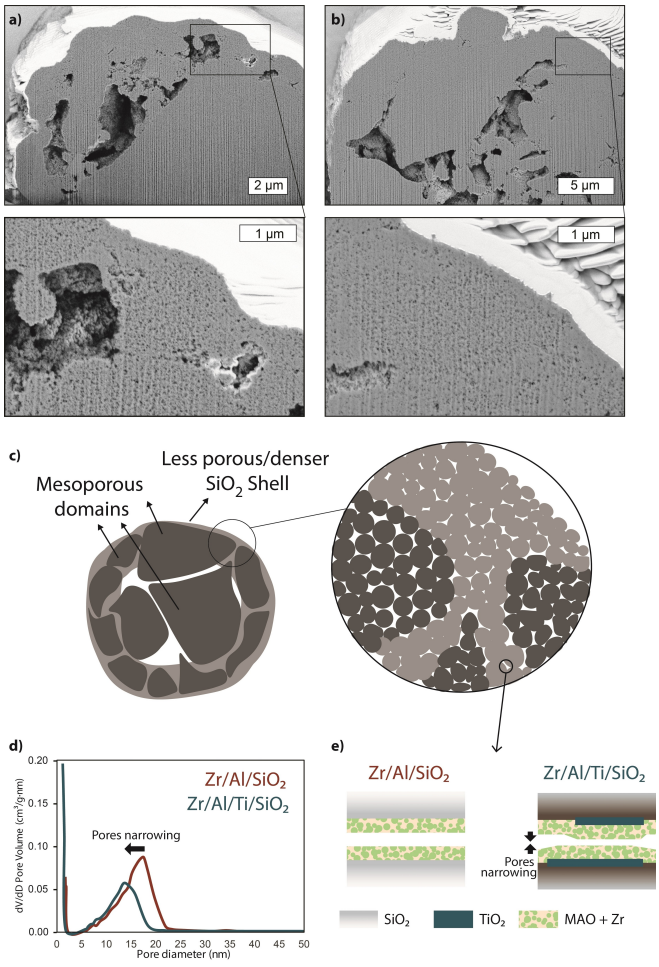

Figure 2. Scanning Electron Microgram (SEM) cross-sections of a pristine a) SiO_2-supported and b) Ti/SiO_2-supported metallocene-based olefin polymerization catalyst particle. In the zoom-in, the two SiO_2 phases with different porosity can be better visualized, namely a denser phase is present in the shell of the catalyst particle, which encapsulates the more porous domains in a spherical catalyst particle. c) Schematic representation of the cross-section of the catalyst particle with the two different silica phases in light and dark grey. d) Barrett-Joyner-Halenda (BJH) desorption curves from N_2-physisorption of $Zr/Al/SiO_2$ and $Zr/Al/Ti/SiO_2$ catalyst materials. e) Schematic representation of the morphology within the pores of the SiO_2 and Ti/SiO_2-based ethylene polymerization catalyst materials.

Results and Discussion

Morphology of pristine catalyst particles

The SiO_2 support material employed in this study is made of an agglomeration of highly mesoporous silica domains, encapsulated by a layer of denser silica a few micrometers thick and interconnected by macropores that run across the core of the particle (Figure 2).[1,8,28] The Ti/SiO_2 support was obtained by adding a titanium alkoxide solution to the SiO_2 support material, followed by a heat treatment step, which resulted in TiO_2 being grafted on the surface Si–OH groups. Though such differences could not be seen from the SEM of the two samples' cross-sections, N_2 physisorption measurements showed that the TiO_2 layer reduced the average pore size from 24 to 22 nm in the bare support and from 17 to 14 nm in the final catalyst, with a corresponding decrease of pore volume (Table 1). Fourier-Transform Infrared spectroscopy (FTIR) on this material also showed that a portion of the isolated Si-OH surface sites present within the commercial silica were replaced by Ti–OH groups.[25] In addition, using CO as a probe molecule in combination with FTIR, it was revealed that multiple neighboring 5-coordinated Ti^{4+} sites were present on this material, as well as a low percentage of 4-coordinated Ti^{4+} sites.[25]

These observations indicate that the TiO_2 was present as a (somewhat discontinuous) layer in the pore walls of the support particles, as depicted in Figure 2e. The porosity change is relevant when considering catalyst particle fragmentation, as a diminished pore volume could lead to accumulation of higher stress on the particle per equal amount of polymer formed, potentially causing an earlier fragmentation of the catalyst. Ethylene polymerization activities measured in the slurry phase, at 9 bar of pressure and room temperature, confirmed that the Ti/SiO_2-supported catalysts material had reached a yield of

Table 1. Ti, Al and Zr content from Inductively Coupled Plasma-Optical Emission Spectroscopy (ICP-OES) analysis and Brunauer-Emmett-Teller (BET) surface areas, total pore volumes and average pore sizes from N_2-physisorption analysis.

Sample	Ti (wt.%)[a]	Al (wt.%)	Zr (wt.%)	Al/Zr molar ratio	BET surface area [m^2/g]	Tot. pore volume[b] [cm^3/g]	Pore size[c] [nm]	Activity[d] [KgPE/molZr*h]
SiO_2	–	–	–	–	231	1.45	24	–
Ti/SiO_2	3.54	–	–	–	241	1.37	22	–
$Zr/Al/SiO_2$	–	12.13	0.43	95	260	0.67	17, <2	1990
$Zr/Al/Ti/SiO_2$	2.21	14.25	0.43	112	295	0.55	14, <2	2700

[a] Ti wt.% is lower in Al containing samples because of the 60% specific mass increase due to methylaluminoxane (MAO) addition. [b] Barret-Joyner-Halenda (BJH) desorption. [c] Pore size at BJH curve maxima. [d] Yield of polyethylene (PE) obtained in slurry-phase reaction at 9 bar of ethylene pressure, 55 °C in 1 h.

polyethylene (PE) after 1 h of reaction 35% higher than that obtained by the catalyst supported on the commercial silica material (Table 1). Part 1 of this work discussed the role played by surface Ti species in the olefin polymerization activation efficiency,[25] while here the focus is on the differences in the catalyst particle fragmentation processes between the two distinct olefin polymerization systems. To make this possible, the ethylene polymerization reactions were performed with the commercial SiO_2 and the Ti/SiO_2-supported metallocene catalyst materials at a series of different reaction conditions. The resulting morphologies and catalyst particle fragmentation behaviors were then observed via FIB-SEM analysis and the 2D cross-section were segmented into polymer, catalyst and macropores regions, in order to quantify them.

Morphology of polymerized catalyst particles and their fragmentation behavior

Because the starting material for both types of ethylene polymerization catalysts was the same commercial silica, the fragmentation mode of the two systems was expected to be generally the same, and analog to that reported for the same commercial silica-supported material.[19]

That is, a predominant layer-by-layer fragmentation at the two main polymerization fronts, being the outer surface and the inner mesoporous silica domains. Nonetheless, though the differences in fragmentation between the two catalyst materials might be subtle, they could be crucial to underline the effect that Ti has on the catalyst activity and are here discussed for each reaction condition employed.

When the SiO_2-supported catalyst material was exposed to 1 bar pressure of ethylene in the gas phase, the polymer accumulated primarily on the particle surface and within the macropore walls, peeling off the catalyst in a layer-by-layer mode (Figure 3a), while mesopores further away from these two fronts were yet to be filled with polymer. After 45 min of reaction, the dense silica shell started to present some cracks containing little to no polymer (Figure 3b), as a consequence of the pressure accumulated in the core of the particle. Although the main fragmentation process was still found to be that of layer-by-layer, the occasional occurrence of these cracks can be crucial to maintain monomer diffusion towards the catalyst core and ensure a continuous catalytic activity.

From Figure 3c–d, it is evident that in the Ti-modified catalyst material the general fragmentation process was very similar to that of the SiO_2-based catalysts, with polymer forming at the surface of the catalyst particle and in the macropores, peeling off fragments of the catalyst concentrically. However, several cracks were found to be already forming within the first 15 min of reaction, and were extensively present in each catalyst particle analyzed for the subsequent reaction times. The segmentation analysis reported in Figure 3e–f shows how the occurrence of such cracks affected the macroporosity ratio as ethylene polymerization progressed over time. For the SiO_2-based catalysts, where these cracks were only seldom occurring after 45 min of reaction, the porosity ratio decreased continuously over time as polymer accumulated in the pores. On the other hand, in the Ti/SiO_2 supported catalyst material, the earlier onset of these cracks corresponded to a constant increase in macropores ratio over time, ultimately leading to a macroporosity ratio being more than two-fold that of the unmodified SiO_2-based catalyst after 60 min of ethylene polymerization.

Increasing the ethylene pressure to 9 and 15 bar, lead to a very quick accumulation of a polymer-dense layer on the outer surface of the SiO_2-based catalyst particles, which hindered ethylene diffusion to the inner core (Figure 4a). In our previous work we discussed that the high concentration of ethylene in the gas-phase could cause a gradient of monomer concentration across the particle leading to initial faster rates at sites on the outer surface.[19] Moreover, poor heat removal in the static gas-phase reactor employed could lead to a local surge in temperature, which also contributed to the increase of the polymerization rate on the surface.

As the diffusion of ethylene through the polyethylene layer is calculated to be slower than in mesoporous materials,[29–31] one could argue that ethylene polymerization in the core of the catalyst particle was considerably hampered by the presence of such thick PE shell. Figure 4a–b compares the cross-sections of catalysts based on the SiO_2 and Ti/SiO_2 supports, polymerized at 15 bar in the gas-phase. In both cases the polymer was primarily accumulated on the outside, although more cracks were formed in the Ti/SiO_2 catalysts, with consequently more polymer being present in the macropore space at the core of the catalyst particle. From the segmentation analysis of Figure 4c–d, it is evident that the support modification has led to a marginally better distribution of polymer between outer surface

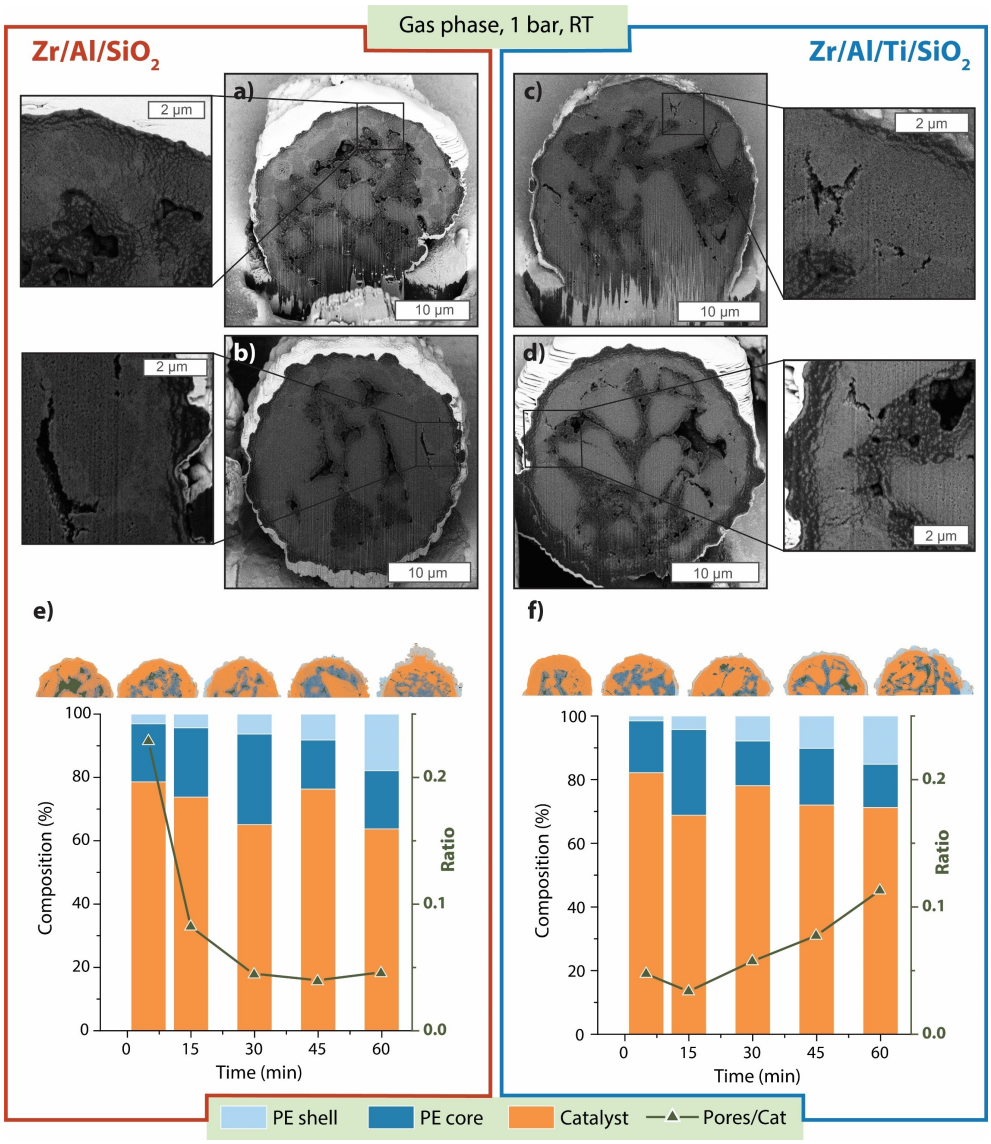

Figure 3. Focused Ion Beam-Scanning Electron Microscopy (FIB-SEM) cross-sections of metallocene-based catalysts polymerized at 1 bar ethylene pressure in the gas-phase and at room temperature. SiO_2-supported catalyst polymerized for a) 15 min and b) for 45 min. Ti/SiO_2-supported catalyst polymerized for c) 15 min and d) for 45 min. Image segmentation analysis of the cross sections of particles reacted for 5 to 60 min e) for the SiO_2-supported catalyst and f) for the Ti/SiO_2-supported catalyst, reporting the trends in polymer, catalyst and macropores ratio in the 2D images.

and macropores, although the overall macroporosity and polymer ratio remained very low for both catalysts. Hence, at these non-ideal conditions the fragmentation was still insufficient to guarantee appropriate catalytic activity in both catalysts, though the modified catalyst propensity to evolve such fractures could still be appreciated (see also Figure S6 for other particles cross sections polymerized at the same reaction conditions).

The effect of introducing a diluent to the reaction mixture was also addressed in our previous work on the fragmentation of SiO_2-based metallocene catalysts.[19] In summary, three main differences were highlighted: first, PE did not accumulate as a thick layer at the outer shell and/or at the macropore walls, but it was found to be more homogeneously distributed as it filled the mesopores from the very beginning of the olefin polymerization reaction; second, catalyst particle fragmentation was more extensive, with a higher contribution of the bisectioning-like fractures which – unlike those found in the gas-phase – were filled with polymer; finally, a certain level of macroporosity was maintained throughout the course of the reaction as catalyst particles expanded. These differences were ascribed to the olefin monomer being more permeable through the heptane-swelled nascent polymer, as well as the better heat dissipation provided by the diluent which prevented the formation of a thicker PE shell. Because mesopores were filled very quickly in the slurry-phase, stress build-up within the silica domains led to polymer-filled transversal fractures, rather than "empty" ones. This was again attributed to the better initial permeability of monomer through the polymer phase, which

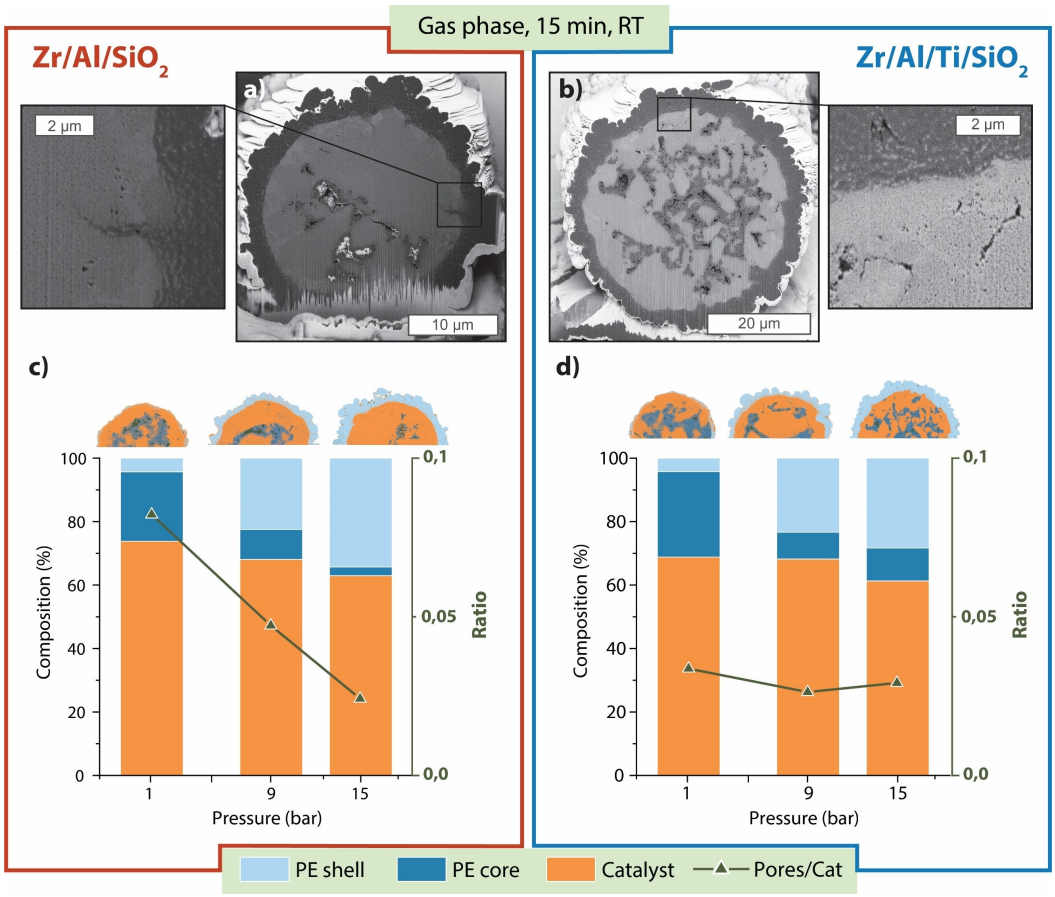

Figure 4. Focused Ion Beam-Scanning Electron Microscopy (FIB-SEM) cross-sections of metallocene-based catalysts polymerized at 15 bar ethylene pressure in the gas-phase for 15 min and at room temperature, a) supported on SiO_2 and b) supported on Ti/SiO_2. Image segmentation analysis of the cross sections of particles reacted for 15 min with increasing ethylene pressure (1, 9 and 15 bar) c) for the SiO_2-supported catalyst and d) for the Ti/SiO_2-supported catalyst, reporting the trends in polymer, catalyst and macropores ratio in the 2D images.

rendered the polymerization rates in the mesopores comparable to the rate of formation of such bisectioning-like cracks.[24,32]

The comparison between the commercial and Ti-modified metallocene-based catalysts, polymerized in the slurry phase at 9 bar of ethylene pressure and room temperature, is found in Figure 5. For the SiO_2-based catalyst material, a thin layer of PE was formed on the outer surface of the particles and at the macropore walls within the first minute (Figure 5a). After 2 min of reaction (Figure 5b) several polymer-filled transversal cracks had appeared, while the concentrical layer-by-layer fragmentation progressed further. This process could be seen to continue over time until small fragments of catalyst were finely dispersed in the polymer phase (Figure 5c). Once again, the general fragmentation behavior of the modified Ti/SiO_2-supported catalyst material looked, at first glance, very similar to that of the commercial catalyst material. However, just like in the gas-phase polymerized catalyst particles, some differences could be found with the presence of a vast number of cracks (not filled with polymer) throughout the dense shell layer of the support material. This could be seen very clearly in the first few minutes of reaction (Figure 5d and e), though such void cracks continued to be present even in the particles reacted for 10 min at these conditions (Figure 5f). This type of fracturing implies a quick release of pressure, which is not followed by an equally fast accumulation of polymer in these newly formed gaps. This could be an indication that for the Ti/SiO_2 supported catalysts the pressure coming from accumulated polymer is higher or that the support dense shell has a different resistance to stress. The segmentation analysis of the cross-section images of the catalyst particles revealed once more that for the Ti-modified catalyst materials, the increase of macroporosity commenced earlier and at a faster pace than that of the commercial SiO_2-based catalyst materials, resulting in more than double the value after 10 min of time at these reaction conditions. Another observation is that the morphology of the outside particle was less smooth for the Ti-modified polymerized catalyst. In fact, the polymer was accumulated in bump-like protrusions, which for the commercial SiO_2-based catalyst material were only occurring in the gas-phase reaction conditions. This phenomenon was ascribed to the fast accumulation of PE on the outer surface of the particles, due to low permeability of olefin monomer through the polymer phase, inefficient dissipation of heat, and a catalyst particle expansion slower than the accumulation of polymer itself, causing the polymer to fold in

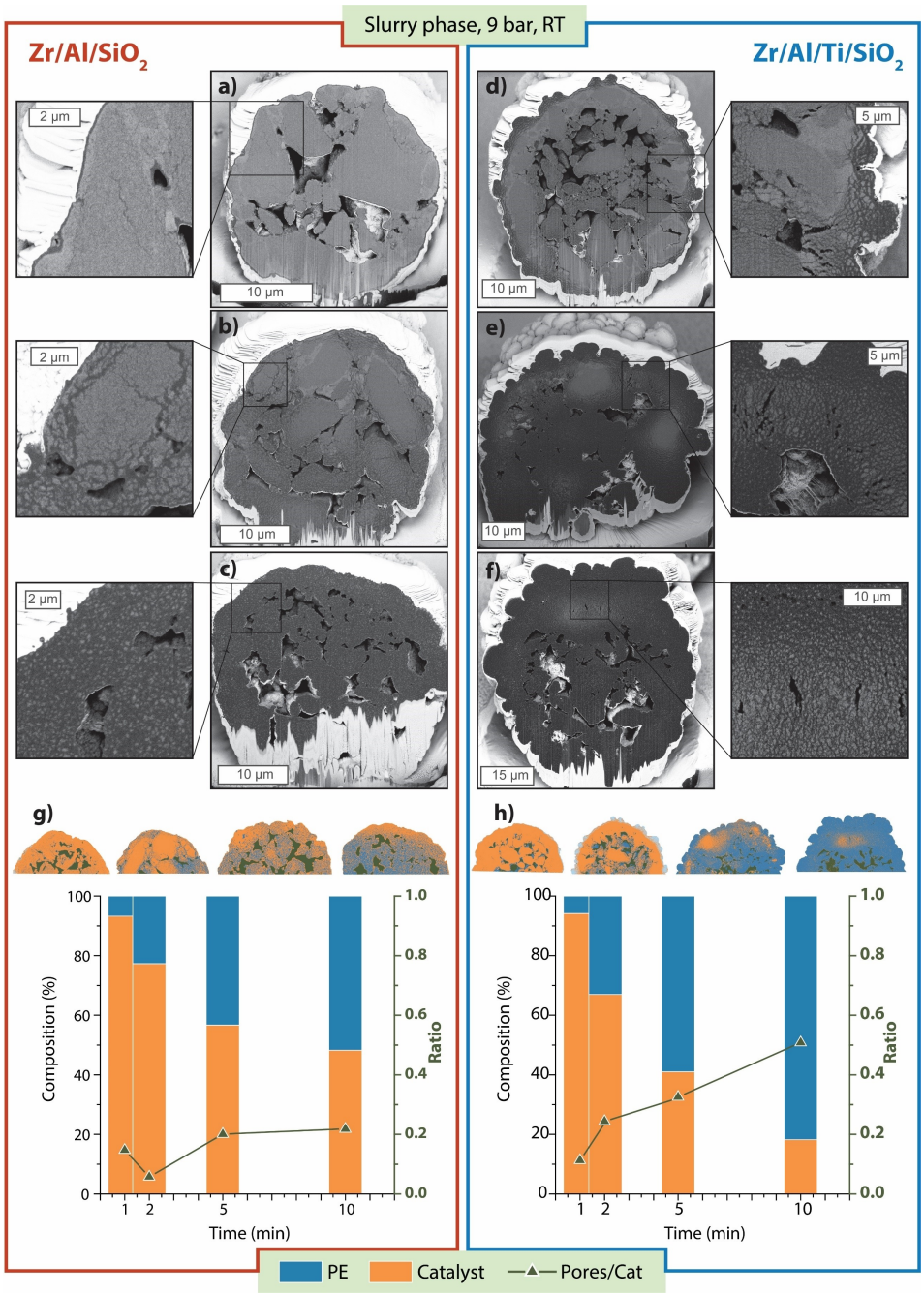

Figure 5. Focused Ion Beam-Scanning Electron Microscopy (FIB-SEM) cross-sections of supported metallocene-based catalysts polymerized at 9 bar ethylene pressure in the slurry-phase with heptane as diluent, and at room temperature. SiO_2-supported catalyst polymerized for a) 1 min, b) 2 min and c) 10 min. Ti/SiO_2-supported catalyst polymerized for d) 2 min, e) 5 min and f) 10 min. Image segmentation analysis of the cross sections of particles reacted from 1 to 10 min g) for the SiO_2-supported catalyst and h) for the Ti/SiO_2-supported catalyst, reporting the trends in polymer, catalyst and macropores ratio in the 2D images.

this manner.[19] In the presence of a diluent the dissipation of heat should be more efficient;[1,3,33] however, as the presence of surface Ti species leads to a more active catalyst, we can argue that here the accumulation of polymer was faster and, despite the increase in macroporosity, it was not accompanied by an equally fast particle expansion. This is an indication of the higher concentration of active sites present in the Ti-modified catalyst.

Finally, the difference in fragmentation with slurry-phase reactions at increasing temperature was also investigated. Elevated temperatures would not benefit the ethylene polymerization reaction kinetics, while milder temperatures could be used to overcome the activation energy barrier.[34] Hence, temperatures up to 60 °C were considered and the resulting particle morphologies of the two catalyst materials under study are shown in Figure 6. Similar to the progress observed at room

Research Article
doi.org/10.1002/cctc.202300222

Chemistry Europe
European Chemical Societies Publishing

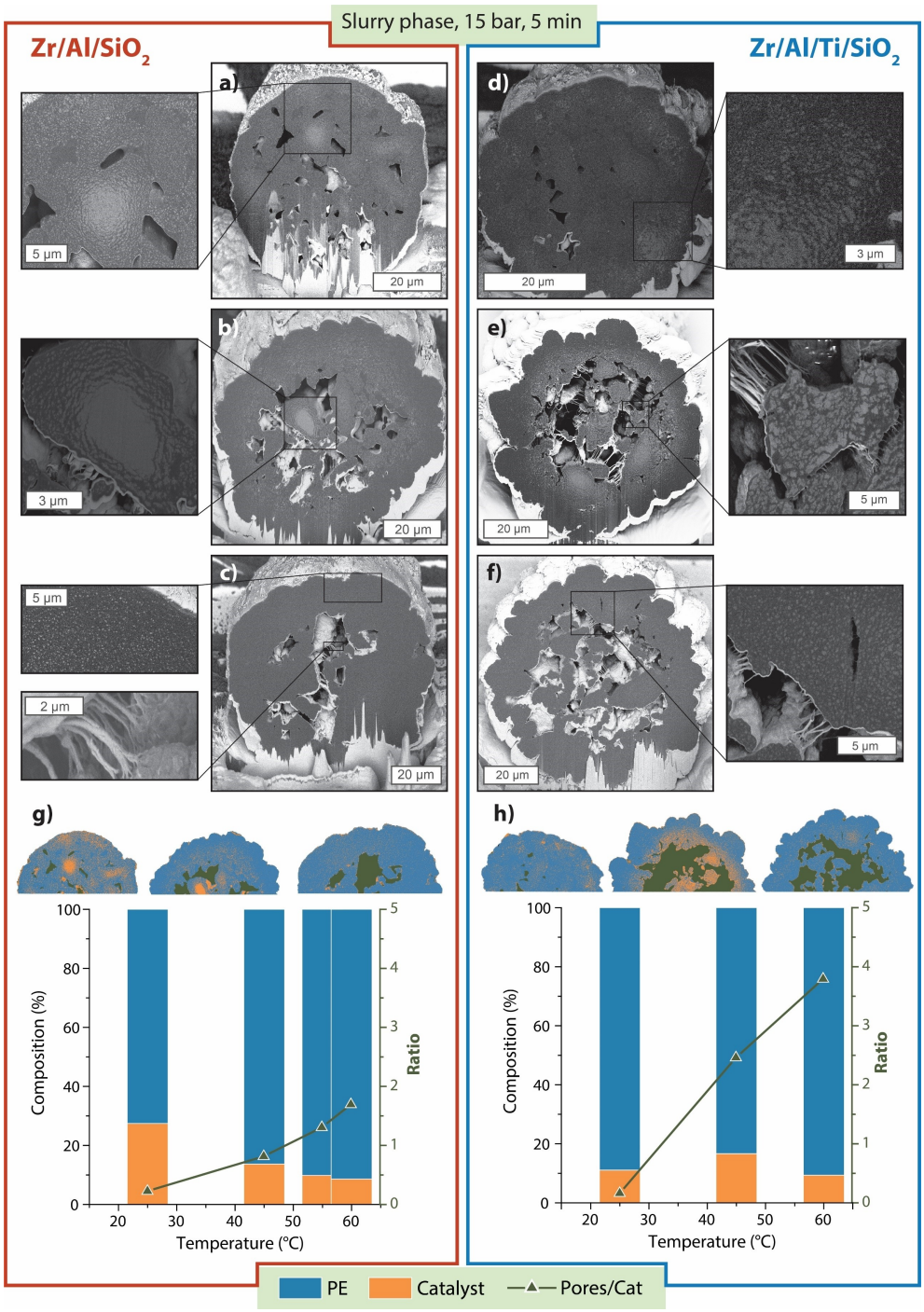

Figure 6. Focused Ion Beam-Scanning Electron Microscopy (FIB-SEM) cross-sections of supported metallocene-based catalysts polymerized at 15 bar ethylene pressure in the slurry-phase with heptane as diluent, for 5 min at different reaction temperatures. SiO_2-supported catalyst polymerized at a) RT, b) 45 °C and c) 60 °C. Ti/SiO_2-supported catalyst polymerized for d) RT, e) 45 °C and f) 60 °C. Image segmentation analysis of the cross sections of particles reacted at increasing temperature g) for the SiO_2-supported catalyst and h) for the Ti/SiO_2-supported catalyst, reporting the trends in polymer, catalyst and macropores ratio in the 2D images.

temperature over time, PE yields increased as a function of reaction temperature and catalyst particle fragmentation proceeded further, while macropores were never completely filled at the reaction temperatures and polymerization times investigated. At these conditions, bisectioning-like transversal fractures were not detected in the commercial SiO_2-based catalyst material (Figure 6a–c), most likely because fragmentation was at an advanced stage where only small fragments of catalyst could be seen embedded in the polymer phase. However, at 60 °C macropores contained thick PE "worm-like" threads connecting different domains (Figure 6c). Similar polymer morphology in the literature has been ascribed to, for example,

the presence of a cluster of active sites, an extrusion-like formation of polymer, a rapid crystallization of the polymer chains, or the occurrence of a rapid axial extension.[21] It is plausible that at these temperatures in the slurry-phase conditions, the polymer crystallization rate caused such polymer conformation to form and to pull strain within the particle, contributing to the particle expansion. Once again, in the Ti-modified supported catalyst, the particles dense shell experienced fragmentation via the formation of transversal cracks which were not filled with polymer (Figure 6e–f). In this sample, polymer fibers could be seen to form at lower temperatures already (45 °C, Figure 6e), though they appeared to be stretched compared to those found in the SiO_2-based catalyst material. This indicates that, after the formation of fibers, the catalyst had expanded pulling them apart. The expansion of the catalyst particles was confirmed by the segmentation analysis (Figure 6g–h), where the macroporosity increase with the reaction temperature was found to be more than two-fold higher for the Ti/SiO_2-based catalyst material than for the unmodified SiO_2-supported catalyst material.

In summary, for the gas-phase and slurry-phase reaction conditions investigated, the Ti-modification of the support material led to an earlier and more extensive fracturing of the support dense shell, evidenced by the appearance of void cracks throughout the outer portion of the particles, accompanied by an overall faster increase of the macroporosity as the fragmentation progressed. This could be due to a different reaction to the stress that is induced by the accumulation of polymer, possibly caused by the morphology changes introduced by the presence of TiO_2 layer in the support mesopores, or due to a different mechanical strength of the Ti/SiO_2 material. Alternatively, these differences could also be ascribed more simply to the faster accumulation of polymer due to the higher concentration of active sites in the modified Ti/SiO_2-based catalyst. To clarify this point, the fragmentation of precursors particles of the modified catalysts, which – as shown in part 1 of this study[25] – were found to also be active for polymerization of ethylene, namely $Al/Ti/SiO_2$, were also analyzed.

Fragmentation of the titanated silica support

The analysis conducted in the previous section showed how the Ti-modified catalyst materials underwent fragmentation during ethylene polymerization with the occurrence of several transversal polymer-free cracks, located on the of cross-section outer portion area and with a more sustained macroporosity that in the polymerized $Zr/Al/SiO_2$ across several reaction conditions tested.

Looking at the activity and porosity data summarized in Table 2, we could argue that the more extensive occurrence of void cracks in the $Zr/Al/Ti/SiO_2$ polymerized catalyst particles could be directly related to 2 factors. Firstly, the ~35% higher polyethylene yields compared to the non-modified $Zr/Al/SiO_2$ would lead to more polymer being accumulated within its pores, leading to such cracking. Secondly, the lower pore volume and narrower pores size in the modified catalyst can be expected to lead to an earlier filling of such pore with comparable amounts of polymer being formed, causing the particles to fracture in this manner.

Table 2. Ethylene polymerization activities of the catalyst materials investigated in this work.

Sample	Activity[a] [gPE/gCat]	Relative activity[b]	Tot. pore volume[c] [cm^3/g]
Al_{TiBA}/SiO_2	–	–	1.45
$Al_{TiBA}/Ti/SiO_2$	25.8 ± 0.2	0.27	1.37
Al_{MAO}/SiO_2	–	–	0.70
$Al_{MAO}/Ti/SiO_2$	23.7 ± 0.2	0.25	0.57
$Zr/Al_{MAO}/SiO_2$	94.7 ± 0.1	1	0.67
$Zr/Al_{MAO}/Ti/SiO_2$	128.6 ± 0.2	1.36	0.55

[a] Yield of polyethylene (PE) per gram of catalyst obtained in heptane slurry-phase reaction at 9 bar of ethylene pressure, 55 °C in 1 h, calculated as average of three measurements [b] Relative activity to that of $Zr/Al/SiO_2$. [c] Barret-Joyner-Halenda (BJH) desorption.

As it was addressed in part 1 of this study, despite the lack of zirconocene active centers, the modified Ti/SiO_2 already possessed some catalytic activity towards the polymerization of ethylene – when in the presence of an Al-based co-catalyst, such as TiBA or MAO, thanks to the presence of Ti species that are activated by Al-based co-catalysts (Table 2).[25] Looking at the fragmentation behavior of this active $Al/Ti/SiO_2$ support could therefore give additional insights in the reasons behind the higher occurrence of transversal cracks and sustain macroporosity in the polymerized $Zr/Al/Ti/SiO_2$ particles when compared to the polymerized $Zr/Al/SiO_2$. The $Al_{TiBA}/Ti/SiO_2$ was chosen, as it has both lower activity and higher porosity than $Zr/Al/Ti/SiO_2$ and $Zr/Al/SiO_2$.

Figure 7a displays the cross-section of a $Al_{TiBA}/Ti/SiO_2$ particle polymerized in the slurry phase at 9 bar of ethylene pressure at room temperature for 5 min. Though the PE yield was very low (< 1gPE/gCat), the dense support shell was already extensively fragmented, including the presence of few empty small cracks. Interestingly, these cracks could be visualized also from the external morphology of all catalyst particles scanned in the polymerized sample, of which one example is shown in Figure 7b.

Figure 7c–d shows the SEM images of cross-sections as well as the outer morphology of the polymerized $Al_{TiBA}/Ti/SiO_2$ particle at higher polymerization yields, obtained at 9 bars for 1 h in slurry-phase conditions and at 55 °C. The macroporosity here was also clearly maintained, several mesopores were also found across the entire particle cross-section, and the outer morphology showed several cracks connected by PE filaments, indicating that these fraction of catalyst material had been drifting apart while polymer grew inside the particle.

Hence, these results show the extensive occurrence of transversal cracks in polymerized $Al_{TiBA}/Ti/SiO_2$, which has a lower activity and a higher porosity than both $Zr/Al/Ti/SiO_2$ and $Zr/Al/SiO_2$. Therefore, this type of fragmentation behavior, being found in both $Al_{TiBA}/Ti/SiO_2$ and $Zr/Al/Ti/SiO_2$, while less so in the $Zr/Al/SiO_2$, is related to the presence of Ti, rather than the higher activity or lower porosity of the $Zr/Al/Ti/SiO_2$ catalyst.

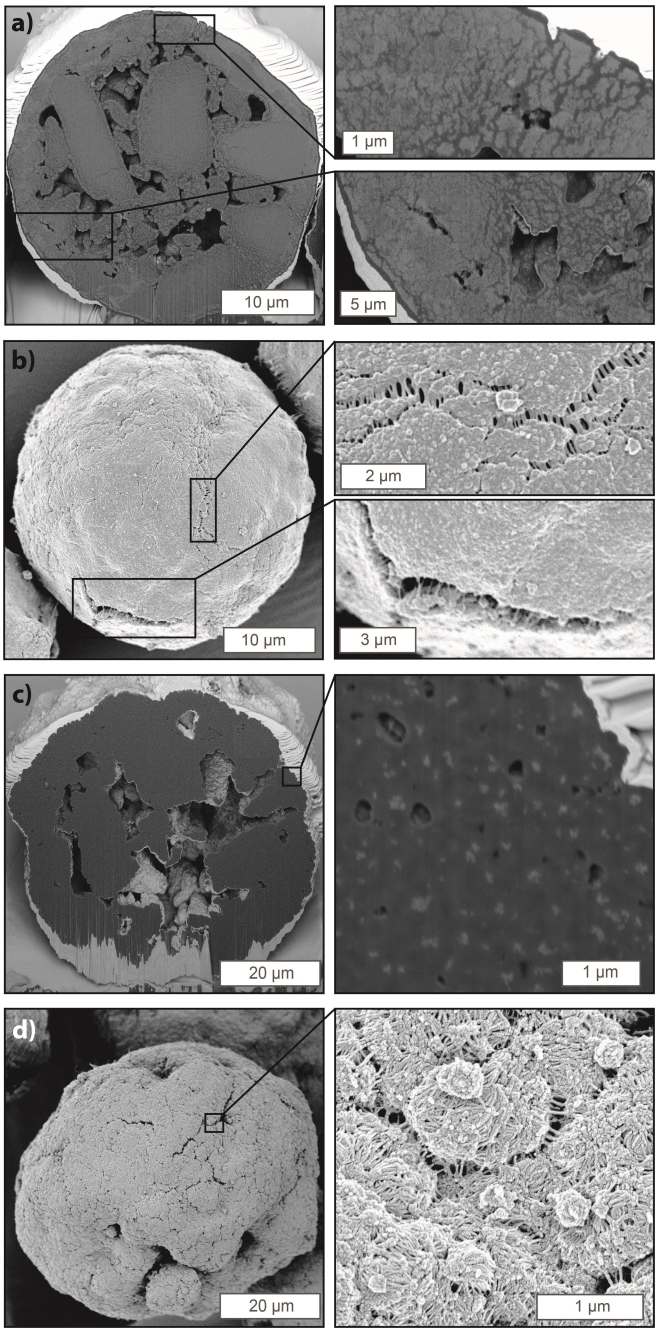

Figure 7. Focused Ion Beam-Scanning Electron Microscopy (FIB-SEM) cross-sections and SEM images of outside morphologies of the $Al_{TiBA}/Ti/SiO_2$ support, polymerized at 9 bar ethylene pressure in the slurry-phase with heptane as diluent, a, b) at room temperature for 5 minutes and c, d) at 55 °C for 1 h.

Having excluded these hypotheses, we suggest that the layer of TiO_2 grafted on the pore walls of the commercial SiO_2 might change the mechanical strength of the mixed metal oxide framework, making it more prone to cracking, well before mesopores become completely filled with polymer. In future work, it would be interesting to measure the mechanical resistance to stress of these samples to further confirm our interpretation of these results.

The differences in the catalyst fragmentation behavior of the two distinct ethylene polymerization catalyst materials under study are schematically represented in Figure 8. In the commercial SiO_2-based metallocene catalyst, small fragments are peeled-off as the ethylene polymerization front proceeds further, while transversal fractures filled with polymer are also occasionally forming – provided that enough pressure is accumulated in the polymer-filled macropores and mesopores. On the other hand, in the modified Ti/SiO_2-supported metallocene catalyst, several polymer-free fractures are present since the very early reaction stages and at all reaction conditions investigated, independently from the degree of PE accumulation in the pores.

Conclusion

The modification of a commercial SiO_2 support by titanation of its surface and pore walls has been shown to offer a support material for metallocene-based ethylene polymerization catalysts with an improved catalytic performance. Part 1 of our study primarily focused on the characterization of the surface species generated after incorporating TiO_2 into the commercial SiO_2-based catalysts which contributed to enhancing its catalytic activity.[25] While the higher amount of active sites in the Ti-modified catalyst was determined to be the primary factor contributing to its superior catalytic performance, the investigation conducted in this second part of the study revealed that this support also facilitated a more efficient fragmentation of the catalyst particles during olefin polymerization, compared to the non-modified catalyst. This conclusion was based on the imaging of more than 40 particles cross-sections of both SiO_2 and Ti/SiO_2 supported metallocene-based catalysts, which were polymerized at different reaction conditions. The main fragmentation mode for both families of catalyst materials was found to be a concentric layer-by-layer peeling of the catalyst particle at the two main fragmentation fronts, i.e., on the outer surface of the particles and at the macropores walls. However, the presence of Ti in the modified SiO_2 support material led to a framework that fractures more easily, as evidenced by the early and extensive formation of void cracks within the catalyst particles analyzed. This phenomenon contributes to a better catalyst fragmentation efficiency as it maintains and adequate diffusion of ethylene across the core of the catalyst particle.

Experimental Section

Catalyst synthesis

Commercial SiO_2 (ES70W, PQ Corporation) was first dried under N_2 flow at 120 °C for 1 h to remove any physisorbed water. The temperature was then raised to 450 °C for 4 h to partially dehydroxylate the silica. Co-catalyst impregnation was performed by mixing the dry silica support to a solution of methylaluminoxane (MAO – 13 wt% Al in toluene, AkzoNobel) for 4 h under reflux, while in an inert atmosphere, with the target loading of 14 wt.% Al. The Al/SiO_2 precursor so obtained was then impregnated with a toluene

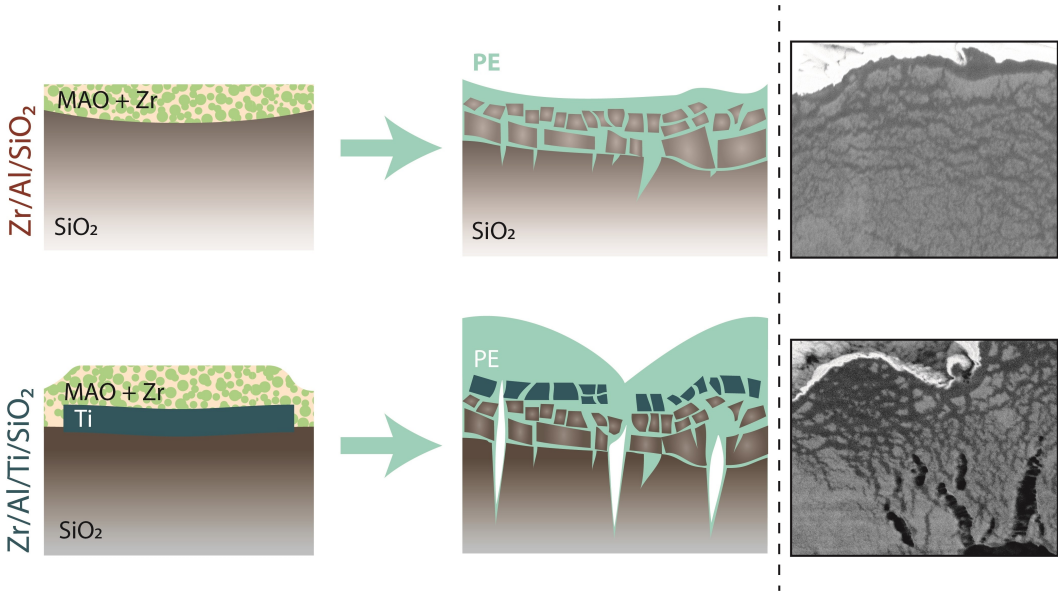

Figure 8. Schematic representation of the pore morphology of metallocene polymerization catalysts supported on SiO_2 (left) and Ti/SiO_2 (right), with corresponding fragmentation process during accumulation of polymer – the methylaluminoxane (MAO) + Zr phase is not depicted in the polymerized scheme for simplicity. The SiO_2-based catalyst fragments mostly in a layer-by-layer mode, while the catalyst supported on the modified Ti/SiO_2 material also fractures with transversal void cracks.

solution of the metallocene catalyst Cp_2ZrMe_2 (Bis(cyclopentadienyl) dimethyl-zirconium(IV) 97%, Sigma Aldrich) for 2 h at room temperature to reach the desired metallocene loading of 1.2 wt.% (0.44 Zr wt.%). After impregnation, the catalyst was filtered and rinsed with dry toluene and pentane (both anhydrous, dried over molecular sieves, Ar, ChemSeal) and then further dried under vacuum to remove remaining solvent traces.

The *Ti/SiO$_2$* support was obtained from the same commercial SiO_2 (ES70W, PQ Corporation), which was first dried at 120 °C for 1 h to remove any physisorbed water and then mixed with a solution of titanium alkoxide (propyl butyl titanate, Tytan™ BIP, Borica Co. Ltd.) in hexane. The solvent was removed from the suspension by evacuation and the remaining Ti impregnated silica was thermally treated at 450 °C for 4 h under nitrogen flow, leading to a 3.5 wt.% Ti content.[35] *Al/Ti/SiO$_2$* and *Zr/Al/Ti/SiO$_2$* were obtained following the same MAO co-catalyst and metallocene impregnation procedures used for the SiO_2-supported samples, as described above.

Catalyst testing

Pre-polymerized catalyst particles were prepared both in the gas-phase and in slurry-phase in a batch autoclave reactor, equipped with an inner quartz vial. The reactor was first loaded in N_2 atmosphere with a few mg of catalyst material and then pressurized with ethylene (i.e., C_2H_4 4.0, Linde). For gas-phase ethylene polymerization experiments, the catalyst was finely dispersed across the quartz vial walls to prevent catalyst deactivation from over-heating and allowing even ethylene access across the sample. For slurry-phase ethylene polymerization experiments, tri-isobutyl aluminum (TiBA, 1.0 M in hexane, Sigma–Aldrich) as impurities scavenger and heptane (n-heptane, anhydrous, over molecular sieves, Ar, ChemSeal) was used as a diluent. All gas-phase ethylene polymerization reactions were performed at room temperature, while the slurry-phase ethylene polymerization reactions were done at temperatures up to 60 °C. Before pressurizing the autoclave reactor, all gas lines were flushed with a series of N_2 and vacuum cycles. Ethylene pressures were varied from 1 up to 15 bar. Reactions were stopped by depressurizing the reactor, after which the polymerized catalyst particles were quenched by addition of ethanol. The quenched catalyst particles were then left drying at room temperature overnight to remove any solvent before weighting the polymer yield and perform FIB-SEM analysis.

Polymerized particles imaging

Samples were loaded on Al stubs with carbon tape and sputter-coated with 10–20 nm of Pt, prior placing them in the electron microscope. Beam currents of 0.1 nA and 2 kV were used to image polymerized catalyst particles with dwell times varying between 10 and 20 µs. External morphologies were imaged by collecting Secondary Electrons (SE) with an Everhart-Thornley detector (ETD), while cross-sections of the catalyst particles were imaged by collecting Back Scattered Electrons (BSE) with a Through-the-Lens Detector (TLD) with a dual Scanning Electron Microscope-Focused Ion Beam (FIB-SEM, FEI Helios NanoLab G3 UC). An extra layer of Pt was deposited on the catalyst particle, at the height where the cross-section was planned to be exposed, via FIB-assisted Pt deposition. Cross-sections were obtained with a Ga FIB, removing half of the catalyst particle material, and then cleaning with precision milling. Discrete, isolated spherical particles were selected for cross-section analysis, based on the observation of a wide range of particles across the sample batch and after estimating average particle size and morphology, to choose a representative particle for each batch. Since micrograms were measured by collecting BSE, the contrast difference depends on the atomic number (Z) of the elements constituting the material they have interacted with.[36] Thanks to the different BSE intensities between catalyst and polymer materials, the cross-sections were segmented in different areas, i.e., each pixel was assigned to either catalyst, macropores, or polymer. Such segmentation was performed in MATLAB with a K-means clustering algorithm, a method of signal processing that categorizes the pixels of the image into *n* clusters in which each pixel belongs to the cluster with the nearest mean (cluster

centroid). More specifically, the pixels assignment to a cluster is based on obtaining the minimum possible sum of the squared distance between the data points and centroid.

Acknowledgements

Coen Mulder and Helen de Waard (Utrecht University, UU) are acknowledged for performing the ICP-OES experiments and Koen Bossers (UU) for the fruitful discussion. The authors acknowledge project funding from TotalEnergies.

Conflict of Interests

The authors declare no conflict of interest.

Data Availability Statement

The data that support the findings of this study are available from the corresponding author upon reasonable request.

Keywords: fragmentation · metallocene · polymerization · support · titania

[1] J. R. Severn, J. C. Chadwick, *Tailor-Made Polymers*, Wiley, Weinheim, **2008**.
[2] F. Machado, E. L. Lima, J. C. Pinto, T. F. L. McKenna, *Polym. Eng. Sci.* **2011**, *51*, 302–310.
[3] J. B. P. Soares, T. F. L. McKenna, *Polyolefin Reaction Engineering*, Wiley-VCH, Weinheim, **2012**.
[4] T. F. L. Mckenna, E. Tioni, M. M. Ranieri, A. Alizadeh, C. Boisson, V. Monteil, *Can. J. Chem. Eng.* **2013**, *91*, 669–686.
[5] M. P. McDaniel, *ACS Catal.* **2011**, *1*, 1394–1407.
[6] T. Vestberg, P. Denifl, C.-E. Wilen, C.-E. Wilén, *J. Appl. Polym. Sci.* **2008**, *110*, 2021–2029.
[7] S. Y. Lee, K. Y. Choi, *Ind. Eng. Chem. Res.* **2012**, *51*, 9742–9749.
[8] G. Fink, B. Steinmetz, J. Zechlin, C. Przybyla, B. Tesche, *Chem. Rev.* **2000**, *100*, 1377–1390.
[9] V. F. Tisse, F. Prades, R. Briquel, C. Boisson, T. F. L. McKenna, *Macromol. Chem. Phys.* **2010**, *211*, 91–102.
[10] X. Zheng, M. Smit, J. C. Chadwick, J. Loos, *Macromolecules* **2005**, *38*, 4673–4678.
[11] R. Goretzki, G. Fink, B. Tesche, B. Steinmetz, R. Rieger, W. Uzick, *J. Polym. Sci. Part A* **1999**, *37*, 677–682.
[12] X. Zheng, J. Loos, *Macromol. Symp.* **2006**, *236*, 249–258.
[13] C. H. Lin, C. Y. Sheu, *Macromol. Rapid Commun.* **2000**, *21*, 1058–1062.
[14] P. Yang, Z. Fu, Z. Fan, *J. Mol. Catal.* **2018**, *447*, 13–20.
[15] F. Ciardelli, A. Altomare, M. Michelotti, *Catal. Today* **1998**, *41*, 149–157.
[16] G. G. Hlatky, *Chem. Rev.* **2000**, *100*, 1347–1376.
[17] A. Köppl, H. G. Alt, *J. Mol. Catal. A* **2001**, *165*, 23–32.
[18] J. C. W. Chien, *Top. Catal.* **1999**, *7*, 23–36.
[19] S. Zanoni, N. Nikolopoulos, A. Welle, A. Vantomme, B. M. Weckhuysen, *Catal. Sci. Technol.* **2021**, *11*, 5335–5348.
[20] A. Yiagopoulos, H. Yiannoulakis, V. Dimos, C. Kiparissides, *Chem. Eng. Sci.* **2001**, *56*, 3979–3995.
[21] A. Di Martino, G. Weickert, T. F. L. McKenna, *Macromol. React. Eng.* **2007**, *1*, 165–184.
[22] J. T. M. Pater, G. Weickert, J. Loos, W. P. M. Van Swaaij, *Chem. Eng. Sci.* **2001**, *56*, 4107–4120.
[23] A. Alizadeh, T. F. L. L. McKenna, *Macromol. React. Eng.* **2018**, *12*, 1700027.
[24] T. F. L. McKenna, A. Di Martino, G. Weickert, J. B. P. Soares, *Macromol. React. Eng.* **2010**, *4*, 40–64.
[25] S. Zanoni, A. Welle, V. Cirriez, B. M. Weckhuysen, *ChemCatChem* **2023**, *15*, e202300221.
[26] K. W. Bossers, R. Valadian, S. Zanoni, R. Smeets, N. Friederichs, J. Garrevoet, F. Meirer, B. M. Weckhuysen, *J. Am. Chem. Soc.* **2020**, *142*, 3691–3695.
[27] K. W. Bossers, R. Valadian, J. Garrevoet, S. van Malderen, R. Chan, N. Friederichs, J. Severn, A. Wilbers, S. Zanoni, M. K. Jongkind, B. M. Weckhuysen, F. Meirer, *JACS Au* **2021**, *1*, 852–864.
[28] K. Cho, H. Chang, D. S. Kil, J. Park, H. D. Jang, H. Y. Sohn, *Aerosol Sci. Technol.* **2009**, *43*, 911–920.
[29] V. Kanellopoulos, E. Tsiliopoulou, G. Dompazis, V. Touloupides, C. Kiparissides, *Ind. Eng. Chem. Res.* **2007**, *46*, 1928–1937.
[30] A. G. Fisch, J. H. Z. dos Santos, N. S. M. Cardozo, A. R. Secchi, *Chem. Eng. Sci.* **2008**, *63*, 3727–3739.
[31] N. M. Ostrovskii, D. Stoiljković, *Theor. Found. Chem. Eng.* **2011**, *45*, 40–52.
[32] P. Smith, H. D. Chanzy, B. P. Rotzinger, *J. Mater. Sci.* **1987**, *22*, 523–531.
[33] M. Ahsan Bashir, T. F. L. McKenna, in *Adv. Polym. Sci.*, Springer, New York, **2017**, pp. 19–63.
[34] M. F. Bergstra, G. Weickert, *Macromol. Mater. Eng.* **2005**, *290*, 610–620.
[35] C. Willocq, A. Vantomme, M. Slawinski, *Modified Catalyst Supports* **2016**, EP2588501B1.
[36] J. I. Goldstein, D. E. Newbury, J. R. Michael, N. W. M. Ritchie, J. H. J. Scott, D. C. Joy, *Scanning Electron Microscopy and X-Ray Microanalysis*, Springer New York, New York, NY, **2018**.

Manuscript received: February 8, 2023
Revised manuscript received: March 14, 2023
Accepted manuscript online: March 22, 2023
Version of record online: May 3, 2023